

L-shell radiative transition rates by selective synchrotron ionization

R D Bonetto¹, A C Carreras², J Trincavelli^{2,3} and G Castellano²

¹ Centro de Investigación y Desarrollo en Ciencias Aplicadas Dr. Jorge J. Ronco, CONICET—UNLP, Calle 47 No. 257—Cc 59, (1900) La Plata, Argentina

² Facultad de Matemática, Astronomía y Física, Universidad Nacional de Córdoba, Ciudad Universitaria (5000) Córdoba, Argentina

³ Consejo Nacional de Investigaciones Científicas y Técnicas, Argentina

E-mail: gustavo@quechua.fis.uncor.edu

Received 20 November 2003

Published 17 March 2004

Online at stacks.iop.org/JPhysB/37/1477 (DOI: 10.1088/0953-4075/37/7/009)

Abstract

Relative L-shell radiative transition rates were obtained for a number of decays in Gd, Dy, Er, Yb, Hf, Ta and Re by means of a method for refining atomic and experimental parameters involved in the spectral analysis of x-ray irradiated samples. For this purpose, pure samples were bombarded with monochromatic synchrotron radiation tuning the incident x-ray energy in order to allow selective ionization of the different atomic shells. The results presented are compared to experimental and theoretical values published by other authors. A good general agreement was found and some particular discrepancies are discussed.

1. Introduction

Radiative transition rates from the different occupied atomic states are parameters of interest in the field of atomic physics, and their accurate values are very useful for testing theoretical models for atomic structure descriptions based on self-consistent methods. On the other hand, the relative intensities of characteristic x-ray lines related to radiative transition rates are essential in non-destructive standardless analysis.

Transition rates to K-shell vacancy states were studied by means of theoretical assessments [1, 2] and experimental determinations (see, e.g., [3] or [4]). However, measurements involving L-shell transitions are scarcely available, due to several experimental complications that arise in determining intensities of lines with similar energies.

In the case of L-lines, the emitted intensities depend on the initial vacancy distribution in the subshells, on their possible rearrangement by means of Coster–Kronig transitions [5] and on the relative decay probabilities from the different occupied states. In turn, the initial vacancy distribution in the subshells varies with the excitation mechanism and with the incident energy used in the ionization process. Therefore, relative intensities of lines from

different subshells depend on the experimental conditions of each particular case. Despite this fact, some studies on L-shell radiative decays have been reported (see, e.g., [6]) in which intensity ratios of $L\alpha$, $L\beta$ and $L\gamma$ groups are determined. The energies for these line groups are quite separated, which allows a relatively easy way for the assessment of the corresponding intensities. Nevertheless, these groups contain transitions from different subshells and corrections are necessary to compare with theoretical data. On the other hand, intensity ratios of lines emitted by the same subshell L1, L2 or L3 are absolute parameters useful for the characterization of atomic structures.

Some of the most frequently cited publications devoted to the theoretical prediction [7], experimental determination [8] and tabulation [9, 10] of radiative transition rates involving L-subshells present discrepancies, which arise from experimental uncertainties and from the approximations assumed in the theoretical calculations. Specifically, it has been shown [11–13] that inner-shell radiative transition rates may differ when Babushkin gauge [14–16] is used instead of Coulomb gauge in the numerical assessments. In addition, discrepancies were reported in the prediction of K-shell radiative transition rates due to the different choice in the way of generating the one-electron wavefunctions [13]. Therefore, it is desirable to count on reliable experimental values in order to support either formalism. On the other hand, data presented by the CRC Press in 1998 [9], widely used in the literature nowadays, were taken from a previous work published by Salem *et al* [8]. Those data were, in turn, assessed by averaging a large set of scattered experimental data measured from 1925 to 1974. In view of the few up-to-date values available, new experimental determinations would mean an important contribution to atomic databases.

Spectral deconvolution is the main problem that arises when determining L-line intensities with energy dispersive systems due to strong peak overlapping. Good statistics is not enough to overcome this problem, and a careful fitting methodology is required in order to produce accurate values for peak areas. Alternatively, radiative transition rates normalized to unity may be obtained with the method of parameter refinement previously developed for electron probe microanalysis (EPMA) [17] and x-ray fluorescence (XRF) [18]. Basically, this method consists in minimizing the differences between experimental and parametrized spectra by optimizing the atomic and experimental parameters involved. Details about the refinement procedure will be given in section 2.

No previous attempt has been reported on the use of selective ionization of subshells in order to assess L-shell transition rates by parameter refinement. This strategy supports the reliability of the results obtained, since the number of parameters to refine in each spectrum is reduced, and the uncertainties due to line overlapping are strongly diminished. In this work, normalized radiative decay rates for L-lines are obtained for a set of seven elements with atomic numbers between 64 and 75, by using the method of parameter refinement mentioned above [18]. The analysed spectra were recorded by means of a synchrotron radiation XRF experiment. For each element, normalized radiative decay rates for L3, L2 and L1 groups were determined by fitting respectively L3, L2–L3 and L1–L3 spectra, using in the last two cases the values obtained in the preceding stage. Special efforts were devoted to obtain estimates for the uncertainties (see section 2), since they may be of interest in any further theoretical or experimental application. Finally, results are compared with data from other authors.

2. Description of the method

The experimental and fitted spectra can be thought of as column vectors \mathbf{y} and $\tilde{\mathbf{y}}$, respectively, whose i th component is the intensity for the energy E_i corresponding to the channel i . The

refinement method deals with the whole spectrum, minimizing the quantity

$$\chi^2(\mathbf{p}) = \frac{1}{N - N_p} (\tilde{\mathbf{y}} - \mathbf{y})^T W (\tilde{\mathbf{y}} - \mathbf{y}), \quad (1)$$

where \mathbf{p} is the vector of parameters to be optimized, N is the number of spectrum channels considered and N_p is the number of parameters adjusted. The weight matrix W is symmetric, usually taken as the inverse of the correlation matrix V_y for the experimental intensities.

The dependence of χ^2 on \mathbf{p} occurs through the expression chosen for $\tilde{\mathbf{y}}$. In order to give an adequate description of the spectrum $\tilde{\mathbf{y}}$, the background contribution, characteristic line intensities and detection artefacts must be appropriately described. In the applications presented here, the continuum below the characteristic peaks was always very low, due to the use of a monochromatic incident beam and to the unimportant scattering produced within the sample chamber in vacuum. Therefore, a constant value B was enough for considering the background contribution; in a more general case, a function $B(E_i)$ might be required.

Expressions arising from fundamental parameters [19] were used in order to calculate the intensities for the characteristic lines. In this model, the intensity $P_{j,q}$ of the line q from element j can be written as

$$P_{j,q} = \alpha C_j \frac{N_A \tau_j(E_0)}{A_j} \omega_j f_{j,q} \epsilon_{j,q} \frac{\Delta\Omega}{4\pi} \frac{1 - \exp(-[\mu(E_0) \csc \phi + \mu(E_{j,q}) \csc \psi]t)}{\mu(E_0) \csc \phi + \mu(E_{j,q}) \csc \psi}, \quad (2)$$

where t is the mass thickness of the sample, E_0 is the energy of incident photons, α is a constant proportional to the number of incident photons, C_j is the mass concentration of element j , A_j its atomic weight, N_A is Avogadro's number, $\tau_j(E_0)$ is the photoelectric cross-section for the atomic shell considered of element j at E_0 , ω_j is the fluorescence yield for the shell involved, $f_{j,q}$ is the normalized radiative transition rate related to the observed line q , $\mu(E_0)$ and $\mu(E_{j,q})$ are the mass attenuation coefficients of the sample for the incident and characteristic energy respectively, ϕ and ψ are the incident and take-off angles, $\epsilon_{j,q}$ is the detector efficiency for the corresponding energy and $\Delta\Omega$ is the solid angle subtended by the detector. In equation (2), multiple interactions have not been taken into account, as they were negligible in the samples analysed. In the applications presented in this work, the fluorescence yield, the mass attenuation coefficients and the characteristic line energies were taken from Hubbell [20], Heinrich [21] and Bearden [22], respectively. In order to account for the detector efficiency, the characteristic thicknesses provided by the manufacturer were used.

Spectrum acquisition was carried out by means of a silicon detector, in which a proportional conversion of the incident photons into an electrical pulse is made. This pulse is registered in a multichannel analyser, where linear calibration of energies is performed by means of two parameters: the 'gain' and the 'zero'. Statistical fluctuations in the initial number of excitations produced by arriving photons of a given energy and electronic noise of the amplification process cause a broadened peak. To a first approximation, it can be assumed to have a Gaussian shape given by

$$G_{j,q}(E_i) = \frac{1}{\sqrt{2\pi}\sigma_{j,q}} \exp\left[-\frac{(E_i - E_{j,q})^2}{2\sigma_{j,q}^2}\right].$$

In this equation, the standard deviation is a function of the photon energy given by

$$\sigma_{j,q} = (n^2 + \varepsilon F E_{j,q})^{1/2}, \quad (3)$$

where n is the uncertainty due to the electronic noise, F is the Fano factor and ε is the mean energy required for a single electron-hole pair formation (3.76 eV at 77 K). However, a correction to this Gaussian shape is required since some of the charge carriers produced by

a photon arriving at the detector may be ‘trapped’ before being collected, the output sent to the amplifier corresponding to an energy lower than the original one. This effect, manifested by low-energy tails in asymmetrical peaks, is more important for soft x-ray lines, for which the absorption occurs near the detector surface, between the active volume and the dead layer, where a higher probability of trapping is expected. This artefact is accounted for by means of the Hypermet function [23]

$$H_{j,q}(E_i) = A[G_{j,q}(E_i) + S_{j,q}(E_i) + T_{j,q}(E_i)],$$

where A is a normalization factor, $S_{j,q}(E_i)$ is a step function of height $s_{j,q}$ convoluted by the Gaussian function $G_{j,q}(E_i)$,

$$S_{j,q}(E_i) = s_{j,q} \operatorname{erfc}\left(\frac{E_i - E_{j,q}}{\sqrt{2}\sigma_{j,q}}\right)$$

and $T_{j,q}(E_i)$ is an exponential tail of width $\beta_{j,q}$ and height $t_{j,q}$ convoluted by $G_{j,q}(E_i)$,

$$T_{j,q}(E_i) = t_{j,q} e^{(E_i - E_{j,q})/\beta_{j,q}} \operatorname{erfc}\left(\frac{E_i - E_{j,q}}{\sqrt{2}\sigma_{j,q}} + \frac{\sigma_{j,q}}{\sqrt{2}\beta_{j,q}}\right).$$

The parameters $s_{j,q}$, $t_{j,q}$ and $\beta_{j,q}$ characterize the peak shape, and they are not known *a priori*. They must be refined from a rough initial estimate in order to take into account peak asymmetries. There are some artefacts that have not been considered in this application, since they do not influence the results in the situations studied. This is the case of the ‘escape’ and ‘sum’ peaks and the spurious peak that may appear at 1.739 keV due to the photoelectric absorption of a photon within the dead silicon layer of the detector. In further applications, these effects can be easily incorporated.

Summarizing, the total intensity for channel i is

$$\tilde{y}_i = B + \sum_{j,q} P_{j,q} H_{j,q}(E_i). \quad (4)$$

The components of vector \mathbf{p} , implicit on the right-hand side of equation (4), are the parameters that can be optimized, namely the scaling factors α (equation 2) and B ; the gain and zero of the detection chain; the peak-width factors n and F of equation (3); the radiative transition rates; the fluorescence yields, the photoelectric cross-sections and the mass concentrations of equation (2); the parameters involved in the function $H_{j,q}$ for each peak; the thicknesses associated with the detector efficiency; the transition energies for each decay, etc.

Since the function χ^2 involves the vector \mathbf{p} in a complex way, a robust routine of minimization and a careful strategy for \mathbf{p} -space exploration are required in order to fit the modelled spectrum to the experimental one avoiding local minima. This is a very important issue, since the numerical routine could yield results seemingly correct, which may strongly deviate from the real values. The downhill simplex algorithm [24] was used because it is a powerful minimization method which implements only function evaluations, not derivatives, reducing numerical errors in the way to the minimum. The optimization procedure involves several steps of minimization, refining a different set of parameters each time. The choice of the most adequate set of parameters for each step represents a delicate task that will define the risk of falling in local minima. As a first stage in the routine of minimization followed along this work, the parameters related to peak shape ($s_{j,q}$, $t_{j,q}$ and $\beta_{j,q}$) and width (n and F) due to the detector response were obtained from K-spectra with characteristic energies in the same region as the L-lines of the elements studied. Subsequently, the calibration coefficients were determined from each L-spectrum. Then, from the L3-spectra, the normalized radiative transition rates corresponding to this subshell were assessed for each element, along with

the peak and background scale factors, whereas the parameters obtained for peak shape, detector response and calibration were kept fixed. The same procedure was followed to obtain L2-transition rates from the spectrum containing L2- and L3-lines, keeping the values of L3-decay rates determined in the previous step. Finally, L1-transition probabilities were computed from the spectrum involving all L-lines, by using the L2- and L3-decay rates obtained in the preceding step. The whole process was repeated starting from different initial values, obtaining the same set of final results, which ensures that the minimum found is the global one.

In order to assess the uncertainties in the parameters optimized, the experimental intensities y_i were regarded as stochastic variables obeying Poisson statistics, with mean values $\langle y_i \rangle$ and standard deviations given by $\sigma(y_i) = \sqrt{y_i}$. A linear approximation may be assumed for the intensities \tilde{y} given by equation (4) in the neighbourhood of the vector of 'true' parameters \mathbf{p}^o :

$$\tilde{y} = \tilde{y}(\mathbf{p}^o) + D(\mathbf{p} - \mathbf{p}^o),$$

where

$$D_{ij} = \left(\frac{\partial \tilde{y}_i}{\partial p_j} \right)_{\mathbf{p}^o}.$$

Then

$$\tilde{y} - \mathbf{y} \simeq D\mathbf{p} - \mathbf{u}, \quad \mathbf{u} \equiv \mathbf{y} + D\mathbf{p}^o - \tilde{y}(\mathbf{p}^o),$$

and therefore equation (1) becomes

$$\chi^2(\mathbf{p}) = \frac{1}{N - N_p} \sum_{ij} \left[\left(\sum_k D_{ik} p_k - u_i \right) W_{ij} \left(\sum_\ell D_{j\ell} p_\ell - u_j \right) \right].$$

The sought vector $\hat{\mathbf{p}}$ must satisfy the condition for minimum

$$\left. \frac{\partial \chi^2(\mathbf{p})}{\partial p_m} \right|_{\hat{\mathbf{p}}} = 0 \quad \forall m,$$

which implies

$$\sum_{ij} D_{im} W_{ij} \left(\sum_\ell D_{j\ell} \hat{p}_\ell - u_j \right) + \sum_{ij} \left(\sum_\ell D_{i\ell} \hat{p}_\ell - u_i \right) W_{ij} D_{jm} = 0,$$

where the index k has been replaced by ℓ . Since $W_{ij} = W_{ji}$, this condition is equivalent to

$$\sum_{ij\ell} D_{im} W_{ij} D_{j\ell} \hat{p}_\ell - \sum_{ij} D_{im} W_{ij} u_j = 0.$$

The first term is the m th component of the vector $(D^T W D) \hat{\mathbf{p}}$, whereas the second is the m th component of $D^T W \mathbf{u}$, from where

$$\hat{\mathbf{p}} = (D^T W D)^{-1} D^T W \mathbf{u}.$$

Thus

$$\hat{\mathbf{p}} = M\mathbf{y} + C,$$

with $M \equiv (D^T W D)^{-1} D^T W$ and $C \equiv M D \mathbf{p}^o - M \tilde{y}(\mathbf{p}^o)$. Since \mathbf{y} is a stochastic variable, so is \mathbf{p} , and the importance of the linear relationship found between them is that it allows a straightforward assessment of the correlation matrix V_p for the parameters p_j . Assuming that the mean value for the minimizing vector of parameters $\langle \hat{\mathbf{p}} \rangle$ is a good estimate for the true set of parameters \mathbf{p}^o :

$$V_p = \langle (\hat{\mathbf{p}} - \mathbf{p}^o)(\hat{\mathbf{p}} - \mathbf{p}^o)^T \rangle.$$

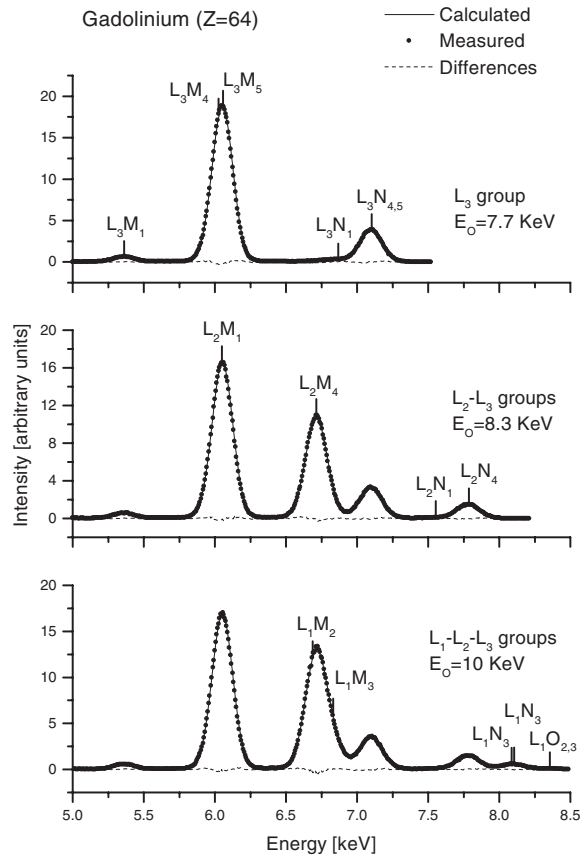


Figure 1. Experimental and fitted spectra for Gd obtained by selective excitation.

Table 1. Experimental conditions for the different samples measured.

Z	Element	E ₀ (keV)		Thickness (cm)	
64	Gd	7.7	8.3	10.0	0.0127
66	Dy	8.3	8.9	11.0	0.0250
68	Er	8.8	9.7	10.2	0.0258
70	Yb	9.4	10.4	11.0	0.0100
72	Hf	10.0	11.2	14.0	0.0254
73	Ta	10.4	11.6	12.2	0.0127
75	Re	11.0	12.45	13.0	0.0250

Writing the right-hand member in terms of \mathbf{y} , and bearing in mind that M is a constant matrix,

$$V_p = M V_y M^T,$$

or equivalently, taking $W = V_y^{-1}$,

$$V_p = (D^T V_y^{-1} D)^{-1}.$$

Since the measured intensities y_i are assumed to be uncorrelated variables, its variance-covariance matrix V_y is diagonal. The last equation allows us to evaluate the uncertainties

Table 2. Normalized transition rates for Gd L-shell.

Transition	This work	Reference [9]	Reference [10]	
α_1	L ₃ M ₅	0.735 ± 0.011	0.7273	0.7155
α_2	L ₃ M ₄	0.075 ± 0.012	0.0810	0.0809
$\beta_{2,15}$	L ₃ N _{4,5}	0.1447 ± 0.0013	0.1515	0.1352
ℓ	L ₃ M ₁	0.0316 ± 0.0012	0.0305	0.0582
β_6	L ₃ N ₁	0.0116 ± 0.0014	0.0072	0.0078
β_1	L ₂ M ₄	0.8413 ± 0.0024	0.8315	0.8188
γ_1	L ₂ N ₄	0.1430 ± 0.0013	0.1413	0.1438
η	L ₂ M ₁	0.0081 ± 0.0017	0.0195	0.0298
γ_5	L ₂ N ₁	0.0057 ± 0.0012		0.0058
β_3	L ₁ M ₃	0.486 ± 0.013	0.4560	0.4464
β_4	L ₁ M ₂	0.247 ± 0.015	0.2772	0.3129
γ_3	L ₁ N ₃	0.118 ± 0.029	0.1231	0.1104
γ_2	L ₁ N ₂	0.093 ± 0.026	0.0876	0.0742

Table 3. Normalized transition rates for Dy L-shell.

Transition	This work	Reference [9]	Reference [10]	
α_1	L ₃ M ₅	0.7288 ± 0.0077	0.7283	0.7177
α_2	L ₃ M ₄	0.0806 ± 0.0077	0.0811	0.0812
$\beta_{2,15}$	L ₃ N _{4,5}	0.145 61 ± 0.000 93	0.1493	0.1350
ℓ	L ₃ M ₁	0.031 46 ± 0.000 77	0.0310	0.0555
β_6	L ₃ N ₁	0.010 97 ± 0.000 84	0.0077	0.0079
β_1	L ₂ M ₄	0.8189 ± 0.0031	0.8294	0.8207
γ_1	L ₂ N ₄	0.1466 ± 0.0010	0.1443	0.1440
γ_5	L ₂ N ₁	0.004 724 ± 0.000 037		0.0057
β_3	L ₁ M ₃	0.489 ± 0.022	0.4500	0.4410
β_4	L ₁ M ₂	0.241 ± 0.025	0.2781	0.3163
γ_3	L ₁ N ₃	0.115 ± 0.038	0.1260	0.1093
γ_2	L ₁ N ₂	0.096 ± 0.038	0.0878	0.0752

Table 4. Normalized transition rates for Er L-shell.

Transition	This work	Reference [9]	Reference [10]	
α_1	L ₃ M ₅	0.7324 ± 0.0066	0.7298	0.7187
α_2	L ₃ M ₄	0.0740 ± 0.0064	0.0814	0.0814
$\beta_{2,15}$	L ₃ N _{4,5}	0.147 99 ± 0.000 82	0.1463	0.1359
ℓ	L ₃ M ₁	0.031 84 ± 0.000 85	0.0316	0.0532
β_6	L ₃ N ₁	0.011 05 ± 0.000 76	0.0082	0.0082
β_1	L ₂ M ₄	0.8213 ± 0.0032	0.8272	0.8210
γ_1	L ₂ N ₄	0.1511 ± 0.0017	0.1473	0.1451
η	L ₂ M ₁	0.0189 ± 0.0030	0.0179	0.0261
γ_5	L ₂ N ₁	0.0067 ± 0.0011		0.0056
β_3	L ₁ M ₃	0.499 ± 0.017	0.4424	0.4348
β_4	L ₁ M ₂	0.248 ± 0.018	0.2810	0.3196
γ_3	L ₁ N ₃	0.133 ± 0.012	0.1283	0.1087
γ_2	L ₁ N ₂	0.0597 ± 0.0076	0.0876	0.0764

$\sigma(p_j)$ as the square roots of the diagonal elements $(V_p)_{jj}$. The matrix elements of D are estimated as the numerical derivatives evaluated in the vector \hat{p} produced by the minimization procedure.

Table 5. Normalized transition rates for Yb L-shell.

Transition	This work	Reference [9]	Reference [10]	Reference [7]	
α_1	L ₃ M ₅	0.7287 ± 0.0059	0.7322	0.7196	0.7249
α_2	L ₃ M ₄	0.0776 ± 0.0056	0.0817	0.0815	0.0823
$\beta_{2,15}$	L ₃ N _{4,5}	0.148 10 ± 0.000 80	0.1420	0.1366	0.1459
ℓ	L ₃ M ₁	0.031 98 ± 0.000 77	0.0327	0.0511	0.0359
β_6	L ₃ N ₁	0.010 80 ± 0.000 61	0.0086	0.0084	0.0085
β_1	L ₂ M ₄	0.8203 ± 0.0029	0.8251	0.8213	0.8160
γ_1	L ₂ N ₄	0.1493 ± 0.0016	0.1499	0.1463	0.1542
η	L ₂ M ₁	0.0222 ± 0.0025	0.0174	0.0247	0.0223
γ_5	L ₂ N ₁	0.005 91 ± 0.000 72		0.0055	0.0054
β_3	L ₁ M ₃	0.479 ± 0.013	0.4337	0.4282	0.4270
β_4	L ₁ M ₂	0.263 ± 0.015	0.2840	0.3231	0.3203
γ_3	L ₁ N ₃	0.110 ± 0.023	0.1293	0.1078	0.1106
γ_2	L ₁ N ₂	0.084 ± 0.020	0.0897	0.0776	0.0787

Table 6. Normalized transition rates for Hf L-shell.

Transition	This work	Reference [9]	Reference [10]	
α_1	L ₃ M ₅	0.7205 ± 0.0051	0.7194	0.7178
α_2	L ₃ M ₄	0.0794 ± 0.0049	0.0803	0.0813
$\beta_{2,15}$	L ₃ N _{4,5}	0.151 57 ± 0.000 80	0.1534	0.1387
ℓ	L ₃ M ₁	0.033 35 ± 0.000 57	0.0330	0.0492
β_6	L ₃ N ₁	0.010 77 ± 0.000 54	0.0087	0.0086
β_1	L ₂ M ₄	0.8053 ± 0.0019	0.8220	0.8181
γ_1	L ₂ N ₄	0.1571 ± 0.0011	0.1515	0.1488
η	L ₂ M ₁	0.0265 ± 0.0019	0.0171	0.0238
γ_5	L ₂ N ₁	0.0056 ± 0.0012		0.0055
γ_6	L ₂ O ₄	0.003 20 ± 0.000 78		0.0016
β_3	L ₁ M ₃	0.416 ± 0.010	0.4237	0.4193
β_4	L ₁ M ₂	0.308 ± 0.012	0.2872	0.3253
γ_3	L ₁ N ₃	0.116 ± 0.026	0.1300	0.1072
γ_2	L ₁ N ₂	0.094 ± 0.033	0.0898	0.0789
γ_4	L ₁ O _{2,3}	0.0226 ± 0.0034		0.0261

3. Experiment

Spectra were acquired at the XRF-beamline of the Laboratório Nacional de Luz Síncrotron (LNLS, Brazil), in an experimental mount corresponding to conventional 45°–45° geometry. Incident x-ray beams were monochromatized by means of a Si(220) double-crystal monochromator, tuning the ionization energies slightly above each L-absorption edge. A Si(Li) detector with a resolution of 168 eV @ Mn-K α was used for recording spectra. In order to reduce absorption in the air, the samples were mounted in a vacuum chamber at 0.2 mbar, achieving low background radiation, because of the little scattering of the incident and fluorescent x-ray beams.

The measured intensities were corrected by self-absorption effects for both incident and characteristic radiations. On the other hand, since the detector was outside the vacuum area, intensities were corrected for absorption in the kapton window sealing the chamber.

Experimental conditions for the measurements performed are shown in table 1. For the sample thicknesses used the contribution of multiple scattering events was unimportant, as mentioned in section 2.

Table 7. Normalized transition rates for Ta L-shell.

Transition	This work	Reference [10]	Reference [7]
α_1 L ₃ M ₅	0.717 ± 0.013	0.7164	0.7182
α_2 L ₃ M ₄	0.080 ± 0.012	0.0812	0.0816
$\beta_{2,15}$ L ₃ N _{4,5}	0.1538 ± 0.0013	0.1398	0.1490
ℓ L ₃ M ₁	0.032 57 ± 0.000 68	0.0483	0.0370
β_6 L ₃ N ₁	0.0115 ± 0.0019	0.0088	0.0089
β_1 L ₂ M ₄	0.8003 ± 0.0019	0.8159	0.8084
γ_1 L ₂ N ₄	0.1601 ± 0.0014	0.1501	0.1581
η L ₂ M ₁	0.0268 ± 0.0023	0.0234	0.0221
γ_5 L ₂ N ₁	0.0054 ± 0.0015	0.0055	0.0055
γ_6 L ₂ O ₄	0.0050 ± 0.0016	0.0028	0.0036
β_3 L ₁ M ₃	0.4171 ± 0.0093	0.4147	0.4134
β_4 L ₁ M ₂	0.3104 ± 0.0096	0.3263	0.3237
γ_3 L ₁ N ₃	0.110 ± 0.039	0.1069	0.1099
γ_2 L ₁ N ₂	0.090 ± 0.045	0.0797	0.0810
γ_4 L ₁ O _{2,3}	0.0273 ± 0.0044	0.0273	0.0287

Table 8. Normalized transition rates for Re L-shell.

Transition	This work	Reference [10]
α_1 L ₃ M ₅	0.7043 ± 0.0063	0.7125
α_2 L ₃ M ₄	0.0767 ± 0.0061	0.0808
$\beta_{2,15}$ L ₃ N _{4,5}	0.167 83 ± 0.000 84	0.1419
ℓ L ₃ M ₁	0.030 75 ± 0.000 56	0.0472
β_6 L ₃ N ₁	0.010 56 ± 0.000 99	0.0090
β_1 L ₂ M ₄	0.7491 ± 0.0016	0.8109
γ_1 L ₂ N ₄	0.2077 ± 0.0017	0.1527
η L ₂ M ₁	0.0227 ± 0.0014	0.0226
γ_5 L ₂ N ₁	0.006 52 ± 0.000 92	0.0055
γ_6 L ₂ O ₄	0.0115 ± 0.0019	0.0059
β_3 L ₁ M ₃	0.3534 ± 0.0091	0.4052
β_4 L ₁ M ₂	0.3286 ± 0.0084	0.3286
γ_3 L ₁ N ₃	0.126 ± 0.048	0.1064
γ_2 L ₁ N ₂	0.113 ± 0.045	0.0812

4. Results and discussion

The method of parameter refinement described above was applied to the spectra acquired. In each fitting, care has been taken to involve a number of spectral data much larger than the number of parameters refined—typically, 40 times larger. As an example, figure 1 shows L₃, L₂–L₃ and L₁–L₃ measured and fitted spectra for gadolinium as well as the differences between them. The method of selective excitation allowed the assessment of relative transition rates corresponding to very close peaks from different subshells, such as L₁M₃ or L₁M₂ with L₂M₄, which would have been very difficult by fitting the three groups altogether.

The good performance achieved in spectral parametrization results in reliable values for the normalized L-radiative transition rates. Nevertheless, for the weakest peaks, relative uncertainties were rather large; transition rates for which the error estimates were greater than 50% have been disregarded. Tables 2–8 show the relative decay probabilities obtained for Gd, Dy, Er, Yb, Hf, Ta and Re, along with theoretical results given by Scofield [7], experimental values obtained by Salem *et al* [8] and compiled by the CRC Press in 1998 [9], and data

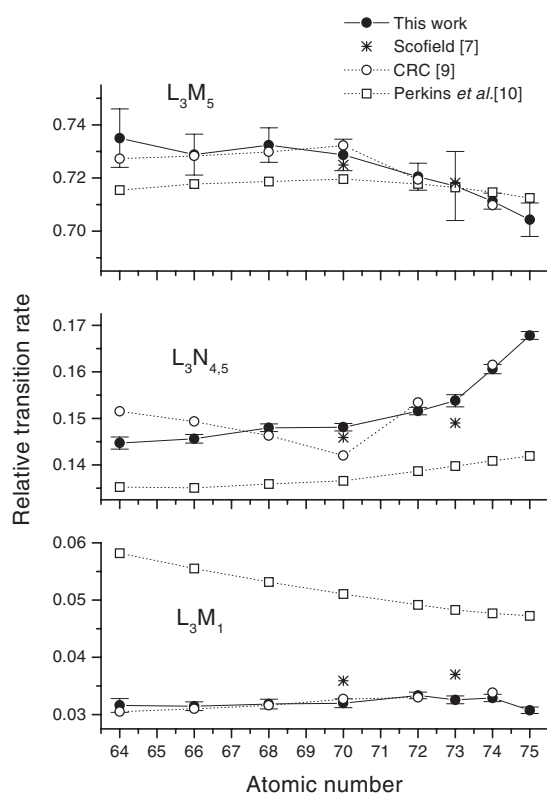


Figure 2. L_3M_5 , $L_3N_{4,5}$ and L_3M_1 relative decay rates obtained in this work as compared to data from the literature.

tabulated by Perkins *et al* [10]. The data published in [9], relative to the most intense line of each group, were normalized to the total amount of radiation generated. Since these data include only the most important transitions for each L-group, the percentage corresponding to the lacking transition rates (typically less than 1% for L3 and L2 groups and around 5% for L1 group) was taken from the results determined here to add up 100%.

As can be seen from tables 2–8, in 74 cases from the 95 transitions displayed, at least two references are available for comparison. In almost 80% of these cases, the results presented are indistinguishable of any of the values given by the other authors, or they do not fall apart from them more than the discrepancy found in the addressed literature. Regarding the precision of the values achieved, around 80% of them exhibit uncertainties lower than 10% or within the spread of the data given by the other authors. The magnitude of the uncertainty for each transition can be understood by observing their relative positions and intensities in figure 1. For instance, considering lines close in energy, such as L_3M_4 and L_3M_5 , the most important relative transition rate can be determined with better precision than the weaker one. On the other hand, transitions such as $L_3N_{4,5}$ or L_3M_1 are determined with low uncertainty although they correspond to weak lines (especially the second one), since they do not present overlapping.

The largest discrepancies with respect to the other authors are mainly found in the L_3N_1 transition (between 18% and 45%) for all the elements analysed. These differences can be attributed to the fact that this transition corresponds to the weakest line considered in the L3 group, and in addition, its energy is very close to that of the $L_3N_{4,5}$ transition. The disagreement

found for the L_2M_1 line of gadolinium is due to its spectral position. Since this peak is mounted on the intense doublet $L_3M_{4,5}$ (see figure 1), it is partially masked by the statistical error.

Some discrepancies in the L_3M_5 , $L_3N_{4,5}$ and L_3M_1 transitions were observed between the present results and the data given by Perkins *et al* [10], for all the studied elements. However, the values obtained here agree with those published in [9], as can be seen in figure 2. Moreover, the transition rates given by Scofield [7] follow apparently the same trend. It can be seen that the results from Perkins *et al* underestimate up to 10% and overestimate up to 100% the general trend for the $L_3N_{4,5}$ and L_3M_1 lines, respectively. It is worth mentioning that, in the relativistic Hartree–Fock–Slater calculations, Scofield [7] took into account the alteration of atomic orbitals before photoemission, whilst Perkins *et al* [10] assumed a frozen-atom scheme, i.e. identical atomic orbitals are allowed in the initial and final states. The importance of exchange and relaxation corrections had already been demonstrated in [1] and [7]. The discrepancies illustrated in figure 2 appear to reconfirm the influence of these corrections.

5. Conclusion

L-shell radiative decay probabilities were obtained for Gd, Dy, Er, Yb, Hf, Ta and Re by means of a method of parameter refinement developed previously for x-ray irradiated samples. The method of selective excitation used together with the parameter optimization algorithm allows us to obtain reliable results even in cases of strongly overlapped peaks belonging to different groups.

In view of the reduced up-to-date information for L-shell radiative transition rates available in the literature, and the discrepancies among the values reported, the results for the 95 decays studied are a useful contribution in the field of atomic physics. In particular, reliable data are necessary to test the performance of different gauges or models for the one-electron wavefunctions in the numerical assessment of radiative decay rates.

The data presented here follow the general trend of those published in the literature. Nevertheless, the values reported by Perkins *et al* [10] show a different behaviour for the L_3M_5 , $L_3N_{4,5}$ and L_3M_1 transitions, as compared to the results obtained in this work and to data given by other authors. On the other hand, more accurate determinations should be provided for the weak transition L_3N_1 . With this aim, the optimization method could be extended to wavelength dispersive spectrometers, which offer better resolution.

Acknowledgments

The authors acknowledge financial support from the Secretaría de Ciencia y Técnica (Universidad Nacional de Córdoba) and the Agencia Córdoba Ciencia S.E. This work was partially performed at the LNLS (Brazil) under proposal XRF 960/01.

References

- [1] Scofield J 1974 *Phys. Rev. A* **9** 1041
- [2] Mukoyama T and Kagawa T 1984 *Phys. Rev. A* **29** 1055
- [3] Dasmahapatra B and Mukherjee A 1995 *Phys. Rev. A* **51** 3546
- [4] Coelho L F S, Gaspar M B and Eichler J 1989 *Phys. Rev. A* **40** 4093
- [5] Bambynek W, Crasemann B, Fink R, Freund H, Mark H, Swift C, Price R and Rao Venugopala P 1972 *Rev. Mod. Phys.* **44** 716
- [6] Ismail A M and Malhi N B 2000 *X-Ray Spectrom.* **29** 317
- [7] Scofield J 1974 *Phys. Rev. A* **10** 1507
- [8] Salem S I, Panossian S L and Krause R A 1974 *At. Data Nucl. Data Tables* **14** 91

-
- [9] Lide D R (ed) 1998 *CRC Handbook of Chemistry and Physics* 79th edn (Boca Raton, FL: CRC Press)
- [10] Perkins S T, Cullen D E, Chen M H, Hubbell J H, Rathkopf J and Scofield J 1991 Tables and graphs of atomic subshells and relaxation data derived from LLNL evaluated atomic data library (EADL) $Z = 1-100$ *Lawrence Livermore National Laboratory Report UCRL-50400* vol 30
- [11] Chen M H and Crasemann B 1983 *Phys. Rev. A* **28** 2829
- [12] Grant I 1974 *J. Phys. B: At. Mol. Phys.* **7** 1458
- [13] Jankowski K and Polasik M 1989 *J. Phys. B: At. Mol. Opt. Phys.* **22** 2369
- [14] Babushkin F A 1962 *Opt. Spectra* **13** 77
- [15] Babushkin F A 1964 *Acta Phys. Pol.* **25** 749
- [16] Babushkin F A 1965 *Opt. Spectra* **19** 1
- [17] Trincavelli J, Castellano G and Bonetto R 2002 *Spectrochim. Acta B* **57** 919
- [18] Carreras A, Bonetto R, Stutz G, Trincavelli J and Castellano G 2002 *X-Ray Spectrom.* **31** 173
- [19] Sherman J 1955 *Spectrochim. Acta* **7** 283
- [20] Hubbell J 1989 National Institute of Standards and Technology, NISTIR 89-4144 (Gaithersburg, MD)
- [21] Heinrich K 1987 *X-Ray Optics and Microanalysis* ed J Brown and R Packwood (Ontario: University of Western Ontario) p 67
- [22] Bearden J A 1967 *Rev. Mod. Phys.* **39** 78
- [23] Phillips G and Marlow K 1976 *Nucl. Instrum. Methods* **137** 525
- [24] Nelder J and Mead R 1965 *Comput. J.* **7** 308